A&A manuscript no.
(will be inserted by hand later)

Your thesaurus codes are:
6(08.01.1; 08.12.1; 13.25.5; 03.13.2)

ASTRONOMY
AND
ASTROPHYSICS
8.7.1997

On coronal abundances derived with the SAX/LECS and ASCA/SIS detectors

F. Favata[1], A. Maggio[2], G. Peres[2], and S. Sciortino[2]

[1] Astrophysics Division – Space Science Department of ESA, ESTEC, Postbus 299, NL-2200 AG Noordwijk, The Netherlands
[2] Istituto e Osservatorio Astronomico di Palermo, Piazza del Parlamento 1, I-90134 Palermo, Italy

Received date 17 April 1997; accepted date

Abstract. We have studied the performance of global χ^2 fitting of low-resolution X-ray spectra in retrieving intrinsic source parameters, with emphasis on the coronal metallicity. The study has been conducted by fitting large numbers of simulated spectra with known characteristics, and studying the distribution of best-fit parameters. We have studied the behavior of the LECS detector on board the SAX satellite and the SIS detector on board the ASCA satellite. The fitted source spectra have either two discrete temperature components or a power-law temperature distribution, with metallicity variations modeled by a single global abundance parameter. The model used for the fitting has always been a two-temperature one, with global varying abundance, to explore the influence of the a priori ignorance of the actual temperature stratification in the source being observed.

The simulations performed explore the influence of varying statistics in the observed spectrum (spanning a realistic range of values) as well as the effect of varying the intrinsic source metallicity, with values in the range 0.15–1.0 times the solar value. We find that the source metallicity can be retrieved within few tens of percent from ASCA/SIS spectra of typical signal to noise ratio, and within few percent from SAX/LECS spectra at the same signal to noise ratio. However relatively small uncertainties in the detector calibrations and in the plasma emission codes are likely to potentially cause large systematic off-sets in the value of the best-fit parameters. Similar systematic off-sets may derive from assuming too simplistic a temperature distribution for the source plasma.

In addition we have re-analyzed the ASCA/SIS spectra of the active giants β Cet and Capella with the same set of assumptions used in the simulations, showing how the best-fit metallicity in these two real cases depends on the details of the fitting process, and in particular on the chosen energy range.

Key words: Stars: abundances; stars: late-type; X-rays: stars; methods: data analysis

Send offprint requests to: F. Favata (ffavata@astro.estec.esa.nl)

1. Introduction

Currently available soft X-ray spectrographs are of the non-dispersive type (CCDs and GSPCs), and the "analysis" of a spectrum, as commonly performed, consists essentially in searching, given a detector response matrix and a plasma emission code, the space of possible "models" (i.e. distributions of temperatures and relative normalizations, as well as elemental abundances), for the "best-fit" one. This is usually done within a set of a priori constraints on the model, in particular fixing the number of discrete temperature components allowed. The usual measure of "goodness of fit" used is the χ^2, and the fitting process thus consists in a search, through χ^2 space, for the model yielding the minimum χ^2 value.

One notable result of X-ray coronal astronomy coming from ASCA is that most (if not all) coronal spectra observed so far with the SIS CCD detector yield, when fit with currently available plasma emission codes, best-fit parameters incompatible with solar (or near-solar) abundance plasmas. At the same time they appear to be "better fit" with elemental abundances typically a fraction of the solar abundance, with values as low as 0.1 times solar not uncommon. This finding points toward a widespread lower-than-solar metal abundance in stellar coronae, although departures from the stellar photospheric abundances, which would be of greater importance, have not been usually investigated.

The limited spectral resolution of non-dispersive X-ray detectors makes it impossible to determine reliably the flux of individual lines or line complexes, so that most studies of coronal abundances up to now have been conducted by doing global fits to the whole spectrum, using the resulting best-fit parameters (including the abundances) as the most probable source parameters. In the presence of complex spectral models, however, it is difficult to assess from first principles what the actual uncertainties related to the fitting process are, and how are the various fit parameters (possibly) correlated with each other.

To help assess the significance of the abundance estimates derived from low-resolution X-ray spectra, as well as to help compare the relative performance of the SIS and LECS instruments for this type of studies, we have performed an extensive set of simulations, to study the sensitivity of the two instruments to variations in the metallicity in the source spectrum, and to assess the relative uncertainties in the derived source parameters. We have first assumed that the source spectrum is intrinsically emitted by two distinct isothermal components, i.e. a so-called "two-temperature" model. This model is bound to be a simplistic representation of a more complicated reality, with the coronal plasma of real stars certainly having a much more complex distribution of temperatures, but the two-temperature model is nevertheless still the work-horse of present day non-dispersive X-ray coronal spectroscopy. Previous work has shown that the spectrum of multi-temperature plasmas confined in coronal loops and yielding a moderate number of counts (as the ones discussed here) may be reasonably well fit by two-temperature models (Ciaravella et al. 1997). This evidence justifies, for the purpose of the present paper, the usage of two-temperature models as "representative" of a more complex reality. The two-temperature source spectra have been fitted with two-temperature models.

As a check for the dependence of the fitting process on the correctness of the assumed source spectrum we have performed an additional set of simulations assuming that the source has a power-law temperature distribution, with spectral index $\alpha = 1.5$ and maximum temperature of 3.0 keV. This type of power-law distribution is reasonably representative, for example, of the emission measure distribution of the solar corona in the temperature range accessible to soft X-ray detectors (Raymond & Doyle 1981). These power-law spectra were fit with the same type of two-temperature models as the two-temperature source spectra, thus simulating our ignorance about the "true" intrinsic source temperature distribution. In the present work the plasma emission model used has been the MEKAL code (Mewe et al. 1995), as implemented in the XSPEC X-ray spectral analysis package (version 9.0)

2. Characteristics of the instruments

The LECS instrument (Parmar et al. 1997) is a drift-less gas scintillation proportional counter with a thin entrance window, providing continuous energy coverage in the spectral range from 0.1 to 10 keV. Its resolution is energy-dependent (varying as $E^{-0.5}$), and becomes comparable to the resolution of the CCD-based SIS detector at $\simeq 0.5$ keV.

The SIS instrument is a CCD-based non-dispersive X-ray spectrometer, providing energy coverage in the band from 0.5 to 10.0 keV, with an approximately constant energy resolution, which is effectively decreasing with time because of the radiation damage of the CCD chip (Dotani et al. 1996). At the time of the launch the effective resolution was $\simeq$ 100 eV at 1 keV, with the precise value depending on the details of the instrumental mode being used. However, the number of spectral resolution elements for the SIS and for the LECS is similar, due to the larger passband of the latter. The spectral resolution of the LECS and of the SIS (at launch) are compared in Fig. 1. We have used a SIS response appropriate for an observation made in early 1995, i.e. two years into operations. This implies a detector performance intermediate between the best possible performance (at launch) and present-day performance.

The effective area of the SIS instrument is, thanks to its bigger mirror, larger than the effective area of the LECS, thus giving it access to fainter sources. The wider passband of the LECS partially compensates, for soft source spectra as the one discussed here, the smaller effective area of the mirrors, so that a given source with the spectral parameters used here yields a comparable count rate both in the SIS and in the LECS. The effective areas of the SIS and of the LECS detector are compared in Fig. 2.

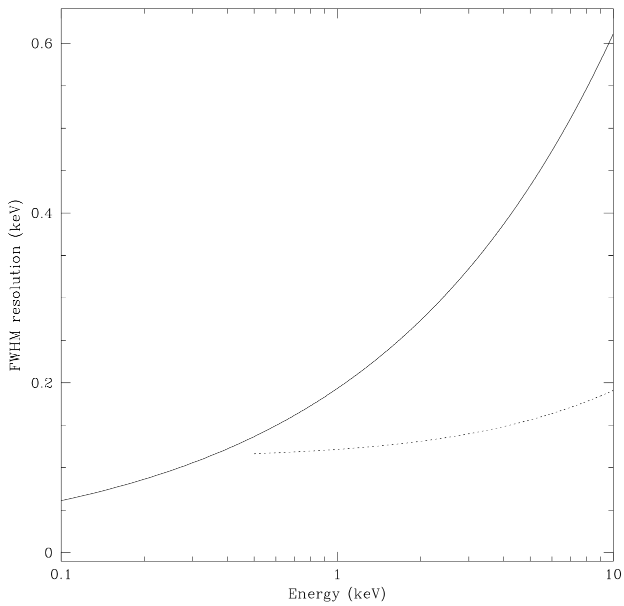

Fig. 1. The full width at half maximum (FWHM) spectral resolution of the SAX/LECS (continuous line) and ASCA/SIS (dashed line) instruments. The SIS resolution is the one at launch time.

3. The simulations

In the first set of simulations a two-temperature source spectrum was used, with temperatures of 0.5 and 2.0 keV, and identical emission measure. Real coronal sources, when modeled with a two-temperature spectrum, display a wide range of parameters, but the values assumed here are reasonably representative of "typical" active stars, as determined, for example, by fitting SIS data. Since the "true" coronal source spectra are likely to be produced by a plasma with a more complex temperature and density distribution, as inferred from spatially-resolved observations of the solar corona, a second set of simulations was performed, using a power-law emission measure distribution with slope $\alpha = 1.5$ and maximum temperature $T_{\max} = 3$ keV for the source spectrum. These parameters are comparable to

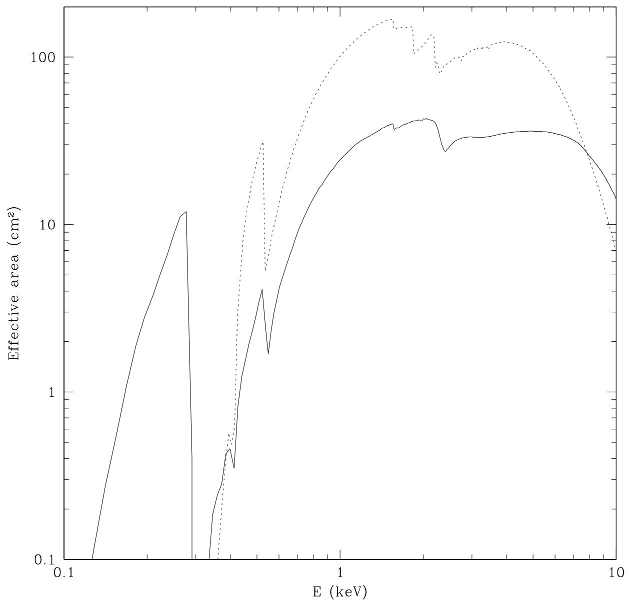

Fig. 2. The effective areas of the SAX/LECS (continuous line) and ASCA/SIS (dashed line) instruments.

those found by Preibisch (1997) when fitting ROSAT/PSPC spectra of field solar-type stars.

The XSPEC package has been used both to produce the simulated spectra and to fit them. 300 realizations of the source spectrum with fixed parameters and with a fixed total number of counts, including statistical errors determined by Poisson statistics were generated. The simulated spectra were then re-binned, so to have at least 20 counts in each resulting new (variable size) energy bin, to ensure that the χ^2 statistics is applicable (Eadie et al. 1971), and each spectrum was fitted, always with a two-temperature MEKAL model, retrieving the best-fit spectral parameters.

The simulations assuming a two-temperature source spectrum were run with 2500, 10 000 and 40 000 source counts, spanning the typical source counts for actual SIS and LECS spectra. The simulations assuming an intrinsic power-law spectrum were all performed with 10 000 source counts. Simulations can supply at most a lower limit to the uncertainty in the derived spectral parameters, because of at least two optimistic assumptions which are only approximations to the reality. First, we are assuming that the MEKAL plasma emission code models describe perfectly the emission from a real plasma, neglecting, among other things, all of the uncertainties in the atomic physics. Second, we are assuming that X-ray detectors are perfectly calibrated, neglecting (possible) systematic uncertainties present in the whole process.

Additionally, we are assuming that the two-temperature model or the power-law emission measure distribution are adequate representations of the source spectrum. On the basis of our knowledge of the solar corona, as well as on the basis of analyses of EUV spectra of real coronal sources, this is likely to be, at best, an approximate parameterization of the coronae of real stars.

Table 1. The numerical experiments performed for the present paper. Two-temperatures source spectra were generated with temperatures of 0.5 and 2.0 keV, and with an emission measure ratio of 1. Power-law spectra have a slope of -1.5 and a maximum temperature of 3.0 keV.

Code	counts	Z	Detector
2-T source spectra			
A2TL0.15	2500	0.15	ASCA/SIS
A2TM0.15	10 000	0.15	ASCA/SIS
A2TH0.15	40 000	0.15	ASCA/SIS
A2TL0.50	2500	0.50	ASCA/SIS
A2TM0.50	10 000	0.50	ASCA/SIS
A2TH0.50	40 000	0.50	ASCA/SIS
A2TL1.00	2500	1.00	ASCA/SIS
A2TM1.00	10 000	1.00	ASCA/SIS
A2TH1.00	40 000	1.00	ASCA/SIS
S2TL0.15	2500	0.15	SAX/LECS
S2TM0.15	10 000	0.15	SAX/LECS
S2TH0.15	40 000	0.15	SAX/LECS
S2TL0.50	2500	0.50	SAX/LECS
S2TM0.50	10 000	0.50	SAX/LECS
S2TH0.50	40 000	0.50	SAX/LECS
S2TL1.00	2500	1.00	SAX/LECS
S2TM1.00	10 000	1.00	SAX/LECS
S2TH1.00	40 000	1.00	SAX/LECS
power-law EM source spectra			
APLM0.15	10 000	0.15	ASCA/SIS
APLM0.50	10 000	0.50	ASCA/SIS
APLM1.00	10 000	1.00	ASCA/SIS
SPLM0.15	10 000	0.15	SAX/LECS
SPLM0.50	10 000	0.50	SAX/LECS
SPLM1.00	10 000	1.00	SAX/LECS

Abundance variations in the source spectrum have been modeled through a single parameter, the global metallicity Z, thus assuming no variations in the abundance ratios with respect to the solar values. In fact, several of the analyses published on SIS spectra of coronal sources result in best-fit spectra with significant variations in the elemental abundance ratios. A simulation-based analysis for the case of individually varying elemental abundances will be the subject of a future paper.

Each numerical experiment is indicated in the following, with a code, and the correspondence between the codes and the experiment parameters is given in Table 1.

4. Simulation results

Each simulation yields a set of best-fit spectral parameters for all the realizations of the sample spectrum. The distribution of the best-fit values is indicative of the uncertainties that can be expected, in the absence of systematic effects, when fitting real spectra with similar statistics.

Some representative cases for the simulations assuming two-temperature source spectra are shown in Figs. 3 and 4, in the form of scatter diagrams, plotting best-fit spectral parameters against each other. For each simulation we have computed the median, as well as the upper and lower 68% and 90% quantiles, corresponding to "1 σ" and "2 σ" levels for each best-fit parameter. The median and quantiles are shown in numerical form in Table 2, and in graphical form in Figs. 5 and 6.

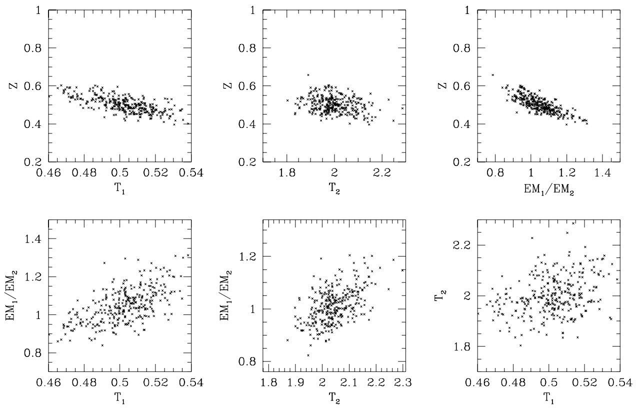

Fig. 3. Two-temperature source spectra fit with two-temperature models: distribution of the best-fit parameters for a set of 300 realizations, with coronal abundance 0.5 times solar as observed with the SAX/LECS detector, with 10 000 counts accumulated per spectrum (experiment S2TM0.50).

4.1. Results for the SAX/LECS two-temperature simulations

Our simulations show that the combination of resolution and spectral coverage offered by the LECS detector allows retrieval of the spectral parameters through a χ^2 fit, for two-temperature spectra, with good accuracy, already for spectra with $\simeq$ 10 000 counts The 2-σ accuracy is $\simeq$ 5% for the source temperatures, and $\simeq$ 15% for the coronal metallicity. LECS spectra with $\simeq$ 40 000 counts allow 2-σ accuracies of $\simeq$ 2% on the source temperatures, and $\simeq$ 7% on the coronal metallicity.

The best-fit parameters show some correlation (Fig. 3), i.e. they appear to be mildly dependent on each other in statistical terms, but the range of variation of the metallicity vs. the emission measure ratio or the temperatures is relatively small. The scatter plots for the rest of the simulations are very similar to the ones in Fig. 3, with the same qualitative features, and a total scatter decreasing as expected with increasing total number of counts, as summarized in Fig. 5. At the same time, as shown in Fig. 6, the relative scatter is essentially independent on the intrinsic source metallicity.

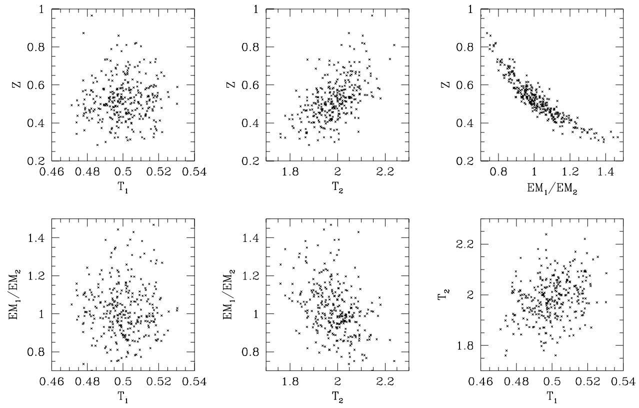

Fig. 4. Two-temperature source spectra fit with two-temperature models: distribution of the best-fit parameters for a set of 300 realizations, with coronal abundance 0.5 times solar as observed with the ASCA/SIS detector, with 10 000 counts accumulated per spectrum (experiment A2TM0.50).

4.2. Results for the ASCA/SIS two-temperature simulations

The results for the simulations relative to the SIS detector differ from the ones relative to the LECS, in the case of two-temperature source spectra fit with two-temperature models, in one important way: the scatter of the best-fit coronal metallicity value is (for the same total number of counts in the spectrum) much larger, as it is the scatter for the best-fit emission-measure ratio. The two are also strongly correlated with each other.

The larger observed scatter implies that while the temperatures can be measured in a $\simeq$ 10 000-counts SIS spectrum with a 2-σ accuracy of $\simeq$ 5%, the coronal metallicity can be measured, in the same spectrum, with a 2-σ accuracy of only $\simeq$ 40%, and an accuracy on the emission-measure ratio of $\simeq$ 25%. Even in the higher statistics spectra ($\simeq$ 40 000 counts), the 2-σ accuracy for the source metallicity is still only $\simeq$ 20%. This, again, in the optimistic assumption of an intrinsic two-temperature source spectrum.

Again, the scatter plots not shown have the same qualitative features of the ones shown, with the total scatter decreasing, as expected, with increasing total number of counts.

4.3. Results for the SAX/LECS power-law simulations

The confidence ranges for the best-fit parameters obtained by fitting a power-law source spectrum with a two-temperature model in the case of the LECS detector are shown in Fig. 7, together with the results relative to the same type of simulations done for the SIS. In this case the confidence ranges are not computed relative to the "true" source parameters (as the source model is different from the model used to fit the data, and thus there are no "true" two temperatures for the source) but rather with respect to the median value found in the simulated set. The only parameter for which the confidence regions are

Table 2. Observed 1- and 2-σ ranges for the best-fit parameters for all the numerical experiments discussed in the present paper. The entries in the table are in percent of the median value of the relevant best-fit parameter.

Code	T_1		T_2		EM_1/EM_2		Z	
	1-σ	2-σ	1-σ	2-σ	1-σ	2-σ	1-σ	2-σ
A2TL0.15	+7 − 7	+13 − 15	+13 − 6	+29 − 12	+74 − 29	+175 − 40	+71 − 44	+114 − 65
A2TM0.15	+3 − 3	+5 − 5	+2 − 4	+5 − 7	+27 − 13	+49 − 23	+24 − 25	+46 − 34
A2TH0.15	+1 − 1	+3 − 3	+0 − 3	+1 − 4	+12 − 5	+21 − 10	+7 − 13	+14 − 21
A2TL0.50	+4 − 4	+7 − 8	+11 − 7	+18 − 11	+35 − 23	+70 − 37	+59 − 32	+131 − 46
A2TM0.50	+2 − 2	+3 − 4	+3 − 4	+6 − 7	+15 − 11	+29 − 18	+25 − 15	+45 − 29
A2TH0.50	+1 − 1	+1 − 2	+0 − 3	+1 − 4	+10 − 2	+14 − 7	+6 − 11	+14 − 16
A2TL1.00	+2 − 2	+4 − 4	+17 − 7	+26 − 14	+36 − 24	+86 − 36	+105 − 32	+214 − 58
A2TM1.00	+1 − 2	+3 − 3	+3 − 5	+6 − 7	+17 − 9	+27 − 16	+28 − 21	+52 − 31
A2TH1.00	+1 − 1	+1 − 1	+0 − 3	+2 − 4	+9 − 3	+14 − 8	+10 − 11	+21 − 18
S2TL0.15	+11 − 11	+16 − 20	+13 − 5	+20 − 11	+37 − 15	+58 − 28	+21 − 19	+58 − 28
S2TM0.15	+5 − 5	+9 − 9	+4 − 4	+7 − 6	+18 − 6	+25 − 13	+10 − 9	+19 − 15
S2TH0.15	+3 − 2	+5 − 4	+0 − 3	+1 − 4	+6 − 4	+12 − 7	+5 − 5	+9 − 8
S2TL0.50	+7 − 5	+10 − 12	+11 − 5	+19 − 10	+26 − 12	+41 − 19	+21 − 17	+42 − 24
S2TM0.50	+3 − 2	+5 − 5	+4 − 3	+6 − 5	+13 − 4	+22 − 9	+8 − 7	+16 − 12
S2TH0.50	+1 − 1	+2 − 3	+0 − 2	+2 − 3	+7 − 2	+10 − 4	+4 − 4	+6 − 7
S2TL1.00	+5 − 5	+8 − 9	+10 − 6	+18 − 10	+20 − 12	+35 − 18	+26 − 17	+49 − 25
S2TM1.00	+2 − 2	+4 − 4	+3 − 3	+6 − 5	+12 − 2	+17 − 7	+10 − 7	+17 − 14
S2TH1.00	+1 − 1	+9 − 7	+3 − 3	+5 − 5	+6 − 0	+9 − 3	+3 − 4	+7 − 7
APLM0.15	+3 − 3	+5 − 5	+4 − 4	+6 − 6	+9 − 8	+15 − 13	+16 − 14	+29 − 21
APLM0.50	+4 − 4	+6 − 7	+4 − 3	+6 − 6	+15 − 10	+23 − 14	+14 − 15	+29 − 24
APLM1.00	+10 − 8	+37 − 11	+4 − 4	+26 − 6	+36 − 22	+403 − 30	+22 − 24	+33 − 60
SPLM0.15	+6 − 4	+9 − 7	+3 − 3	+5 − 5	+18 − 13	+33 − 21	+8 − 9	+14 − 15
SPLM0.50	+6 − 7	+13 − 11	+4 − 3	+9 − 5	+26 − 17	+55 − 28	+11 − 10	+20 − 17
SPLM1.00	+21 − 16	+30 − 29	+19 − 8	+32 − 12	+130 − 43	+234 − 59	+33 − 19	+57 − 28

computed relative to the source value is the metal abundance. Inspection of Fig. 7 and of Table 2 shows that, if the intrinsic source metallicity is really as low as 0.15 times solar, the confidence regions derived by using a two-temperature model are exceedingly broad. We will further discuss only the results relative to the $Z = 1.0$ and $Z = 0.5$ cases.

A comparison of Fig. 6 with Fig. 7 shows that, for the LECS detector, the size of the confidence regions for the best-fit temperatures has increased slightly in comparison with the case of two-temperature source spectra, as it has for the best-fit emission-measure ratio. The best-fit metallicity is also showing slightly larger confidence regions, in addition to a significant offset from its true value, with the two-temperature model retrieving lower abundances than the true value.

4.4. Results for the ASCA/SIS power-law simulations

When the SIS is used to fit power-law source spectra with a two-temperature model, the χ^2 on average does not converge to a satisfactory value. For the cases with $Z = 0.5$ and $Z = 1.0$ the median χ^2 values of the fit are 1.17 and 1.27, respectively, which on account of the large number of degrees of freedom of the fits presented here ($\simeq$ 200) corresponds to fits which are formally unacceptable with a probability (for the $Z = 1$ case) of $\simeq 0.5\%$. This has an influence on the size of the confidence regions, and makes it appear the fitting process to be "more precise" than it actually is. As a result, the confidence regions for this case cannot be directly compared with the previous cases, in all of which the best fit χ^2 distribution did not show any excess above the expected distribution.

The confidence regions for the SIS two-temperature fits of power-law source spectra are still significantly larger than the LECS ones, although they appear (because of the above-mentioned effect) to be smaller than the regions for the two-temperature fitting of two-temperature source spectra (again but for the case $Z = 0.15$, which shows an anomalous scatter). However, the median best-fit metallicity appears to be close to the intrinsic metallicity of the original power-law model.

5. Comparison between the ASCA/SIS and SAX/LECS detectors

The SIS and LECS detectors differ in their trade-offs of resolution and spectral coverage, and thus behave differently in their

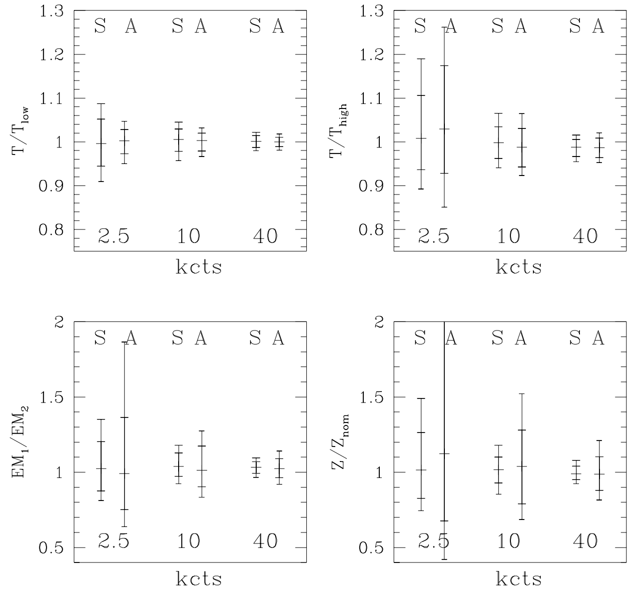

Fig. 5. Two-temperature source spectra fit with two-temperature models: the effect of increasing photon statistics on the 68% and 90% error ranges for the best-fit parameters. Each panel shows the error ranges for a given parameter, with the number of counts in the total spectrum indicated by the bottom label. The top label indicates the instrument ("S" for SAX/LECS and "A" for ASCA/SIS). The two top panels show the error range for the cool (top left) and hot (top right) temperatures, while the bottom panels show the range for the ratio between the two emission measures (bottom left) and for the coronal metallicity (bottom right).

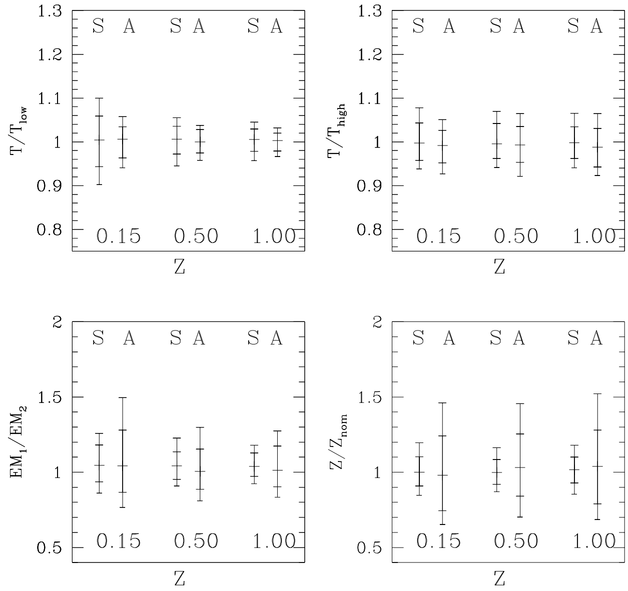

Fig. 6. Two-temperature source spectra fit with two-temperature models: the effect of different source metallicity on the 68% and 90% error ranges for the best-fit parameters, illustrated using the simulations with 10 000 counts in the source spectrum. Each panel shows the error ranges for a given parameter, with the source metallicity indicated by the bottom label. The top label indicates the instrument ("S" for SAX/LECS and "A" for ASCA/SIS). The panels have the same structure as in Fig. 5.

capability to retrieve source parameters, as well as in their sensitivity to discrepancies between the intrinsic source spectral model and the model being used to fit the data.

5.1. Two-temperature intrinsic source spectra

Given the same total number of counts in the spectrum, the SIS detector does a slightly better job in determining the source temperatures, but it performs worse than the LECS in terms of retrieving the coronal metallicity of the source under investigation (Figs. 5 and 6). A solar-metallicity, $\simeq$ 10 000-counts LECS spectrum allows the coronal metallicity to be determined with a 2-σ accuracy of $\pm 15\%$, comparable to the accuracy obtained with a $\simeq$ 40 000-counts SIS spectrum.

The reason for this large difference lies in the diagnostic which is being exploited by the fitting process to derive the abundance. The metallicity is essentially determined by balancing the spectrum in the region between 0.7 and 1.2 keV, where line emission (mostly by Fe L lines) dominates and where the statistics are best, both in the SIS and in the LECS, with the available continuum emission. The region around 1 keV is thus acting as a sort of "pivot" for the fitting process. In the case of the SIS, little continuum is usually available, mostly in the (limited) region between 0.5 and 0.7 keV, in which however the detector's resolution is lowest, and thus the continuum contribution may not be easily disentangled from the nearby line emission. The continuum in the hard tail of the spectrum, typically the small regions between the major K-complexes of heavier elements has, for most coronal sources, low intrinsic source flux, and thus low signal to noise ratio.

For LECS spectra the region below 0.5 keV supplies a very well constrained determination of the continuum, and makes the fitting process much more robust. To confirm the importance of the region below 0.5 keV we have performed an additional set of simulations for the LECS, fitting only the spectrum above 0.5 keV, i.e. using only the information available to the SIS detector. As expected, the performance for the LECS becomes comparable to the performance of the SIS (actually slightly worse, not surprisingly, given its lower spectral resolution). Fig. 9 shows the effect of moving the low-energy cut from 0.1 to 0.5 keV for LECS spectra on the confidence regions, for the sample case of solar-metallicity spectra with 10 000 counts.

5.2. Power-law intrinsic source spectra

When power-law source spectra are fit with two-temperature models, the two detectors discussed here behave differently. While the LECS produces formally acceptable fits, but with

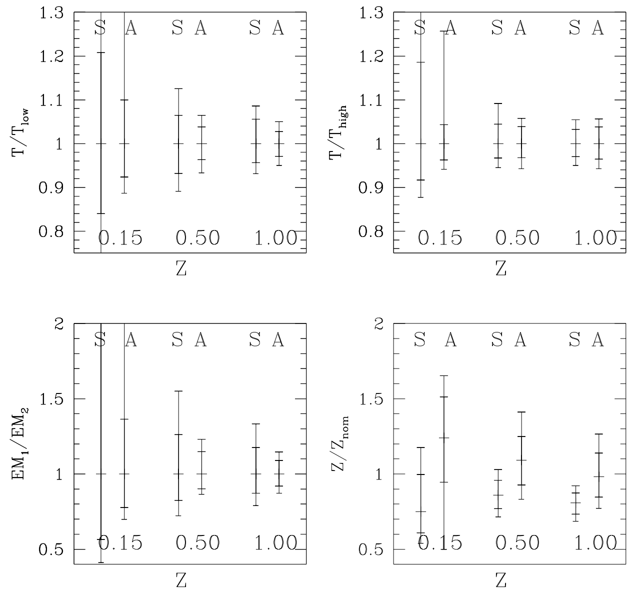

Fig. 7. Power-law emission measure source spectra fit with two-temperature models: the effect of different source metallicity on the 68% and 90% error ranges for the best-fit parameters. Each panel shows the error ranges for a given parameter, with the source metallicity indicated by the bottom label. The top label indicates the instrument ("S" for SAX/LECS and "A" for ASCA/SIS). The panels have the same structure as in Fig. 5.

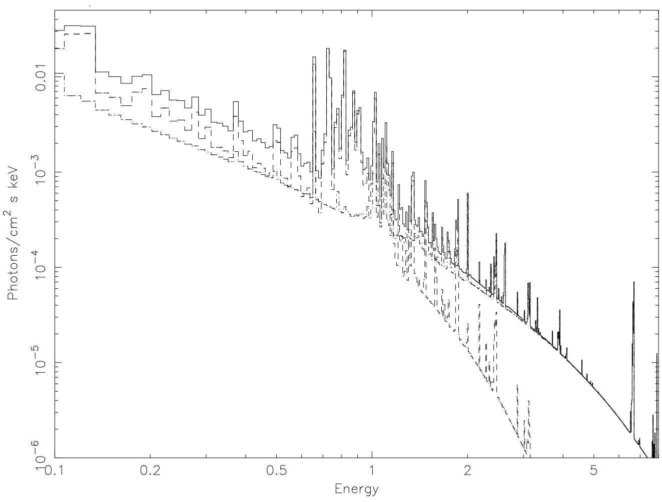

Fig. 8. The two-temperature model source spectrum, for solar abundance, used in the present work. Notice the almost line-free continuum below 0.5 keV, which can be exploited by the SAX/LECS for metallicity determinations and which is not available to the ASCA/SIS. The two dashed lines are the two individual temperature components, while the continuos line is the total spectrum.

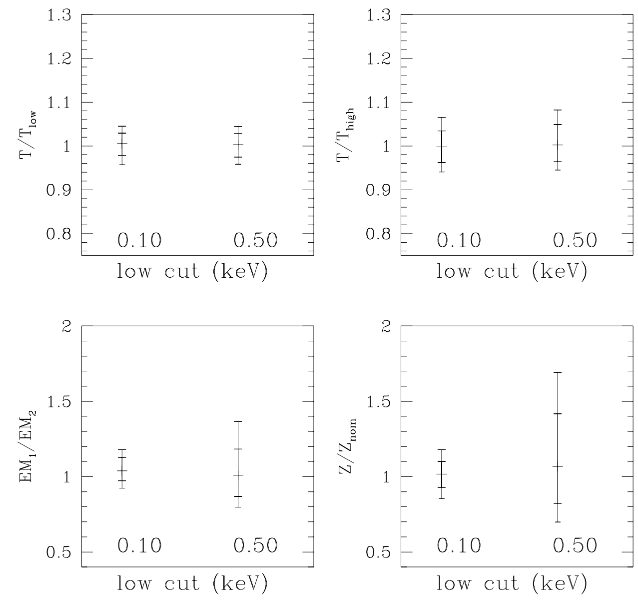

Fig. 9. Two-temperature source spectra fit with two-temperature models: the effect of moving the low-energy cut for SAX/LECS spectra from 0.1 to 0.5 keV is illustrated for the sample case of solar-metallicity spectra with 10 000 counts. The panels have the same structure as in Fig. 5.

lower best-fit metallicities than the intrinsic source value, the SIS detector produce formally unacceptable fits, while still converging on the right source metallicity.

This behavior can be explained as follows: when performing simulations with the same total number of counts for the SIS and the LECS, the smaller energy coverage of the SIS results in a concentration of counts in the $\simeq$ 1 keV region, yielding spectra with higher statistics than in the case of the LECS, in which the counts are spread in a larger spectral region with two distinct peaks (at $\simeq$ 0.2 and $\simeq$ 1 keV), so that the resulting statistics (particularly in the peak channels) are correspondingly lower. This explains why the SIS spectra in this case result, with the same number of total counts, in worse χ^2 values than the LECS ones.

The convergence of LECS spectra on a lower than intrinsic metallicity value is due to a different effect: LECS fits are driven mainly by the balance between the two high-statistics regions of the spectrum, i.e. the continuum below $\simeq$ 0.4 keV and the line-rich region around $\simeq$ 1 keV. When attempting to fit power-law spectra with two-temperature models the discrepancy between the source spectrum and the fitting model is such that the fit is lead to a lower abundance model by the need to balance the lines and the continuum. This does not happen in the case of the SIS, again because of the lack of high-statistics continuum regions.

The reality of the above effect is well shown by a further set of simulations, in which the same LECS power-law source spectra are fit only using the spectral region above 0.5 keV. In this case the fit is "pivoting" around the high-statistics 1 keV region, and is being driven to higher metallicities (this time higher than the intrinsic source metallicity) by the residuals in the high-energy tail. Fig. 10 shows how the confidence regions change when the soft cut in the LECS spectra is moved from 0.1 to 0.5 keV, indicating that when the fitting model is not strictly adhering to the true source thermal distribution the best-fit metallicity can be strongly influenced by the spectral region being used. Conversely, a best-fit metallicity which changes with the spectral region being fit is simptomatic of too simplistic a model. The direction and the size of the effect in real cases will depend on the (a priori unknown) intrinsic source temperature distribution, so that the present case only has an illustrative value.

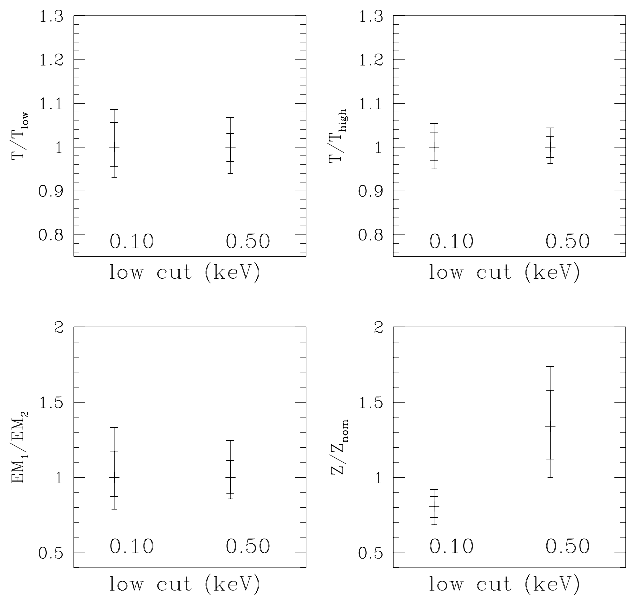

Fig. 10. Power-law emission measure source spectra fit with two-temperature models: the effect of moving the low-energy cut for SAX/LECS spectra from 0.1 to 0.5 keV is illustrated for the sample case of solar-metallicity spectra with 10 000 counts.

6. Two test cases: the observed ASCA/SIS spectra of β Ceti and of Capella

We have analyzed the SIS spectra of the active giant β Cet and of the active binary Capella obtained during the Performance Verification (PV) phase. The data were retrieved from the public archive, and analyzed according to the procedures suggested for ASCA data.

The data for β Cet consist of two segments, of $\simeq$ 8 and $\simeq$ 3.4 ks each, taken in two different instrumental modes (FAINT and BRIGHT mode). They have thus been processed separately, but have been fit simultaneously, as discussed in Maggio et al. (1997). Although the β Cet SIS spectrum is better fit with a model in which the individual abundances are left free to vary (as is the Capella spectrum), for coherence with the simulations, they have been fit here with global varying abundances. Again, we have used the MEKAL emission code as implemented in XSPEC V.9.0; the results therefore are not directly comparable with the ones of Drake et al. (1994), obtained with the MEKA emission code (an earlier version of the MEKAL code, see Mewe et al. 1995 for a description of the changes). Eventual differences in the version of the ASCA pipeline processing may also influence the results. The two resulting spectra have been rebinned at a minimum of 20 cts per bin. The summed number of counts from both spectra was $\simeq$ 10 000.

The β Cet SIS spectrum was first fitted across a broad band, from 0.5 keV up to 4.0 keV. In this energy range the best-fit metallicity is $\simeq$ 0.9 times solar. However, the exclusion of channels at the soft end of the spectrum causes the best-fit metallicity to change, making it decrease to 0.33 solar if channels with energies from 0.5 to 0.6 keV are excluded, and as low as 0.22 if channels up to 0.7 keV are excluded. At the same time, the ratio between the emission measures of the cool and of the hot component increases, showing the same type of behavior as the simulations for the case of intrinsic two-temperature source spectra, where lower best-fit metallicities are correlated with higher emission-measure ratios.

The same type of analysis was done for the Capella spectrum, finding a best-fit abundance for the broad-band (0.5–5.0 keV) SIS Capella PV phase spectrum of 0.54 times solar. As for β Cet, the exclusion of spectral channels below 0.6 keV lowers the best-fit abundance to 0.24 times solar, and exclusion of the channels below 0.7 keV lowers it even more, down to 0.18 times solar. As for β Cet these results are not directly comparable to the ones of Drake (1996).

The χ^2 does not converge, neither for Capella, nor for β Cet to formally acceptable values. The physical meaning of best-fit parameters is thus clearly questionable, and they should not therefore be taken at face value. The strong and systematic dependence of the best-fit metallicity on the spectral region in the Capella and β Cet spectra indicates the presence of some systematic error either in the spectral model used (i.e. the emission code itself, the source temperature structure, the assumption of solar metallicity ratio or a combination of these) or in the detector's calibration (or both).

The continuum region used by the SIS fits (the region between $\simeq$ 0.5 and $\simeq$ 0.75 keV) is almost (but not entirely) line-free, but, at the resolution of the SIS, and given the calibration uncertainty in the region (Dotani et al. 1996) it contains a significant number of source counts "spilling over" from the Fe-L complex. The statistics in this region are, for coronal sources, invariably higher than for the hard tail where line complex from the K-transitions of the heavier elements are visible, and will accordingly influence the metallicity determination.

The increase of the best-fit metallicity with inclusion of a softer spectral region can be explained by assuming that the models being used for the fit (either because of problems in the emissivity models or because of calibration problems, or a mixture of both) have a lack of flux in the region around 1 keV (which is dominated by the cooler temperature component). This could happen, for example, if a number of lines which exist in real spectra were missing from the models. In this case the fit process would converge by balancing the apparent flux deficit around the line-rich 1 keV region. The strategy "chosen" by the fit process will be different depending on the spectral region being fit. If the softer channels are excluded, the fit process can freely increase the cool emission measure to drive up the 1 keV region, while at the same time decreasing the metallicity to avoid discrepancy in the hard tail, dominated by the hot component. If the softer channels are included, however, the high emission measure of the cool component drives up the pseudo-continuum around 0.5 keV, and thus the fit process has to increase the metallicity (to add flux around 1 keV without adding more continuum at 0.5 keV) and correspondingly decrease the emission measure of the soft component. The effect is well visible in the SIS spectrum of β Cet shown in Fig. 11.

We have also fit the same spectra ignoring the region between 0.75 and 1.1 keV. The result reinforces the above conclusions: the best-fit metallicity for the β Cet spectrum rises to 1.1 times solar, the same value which is found for the Capella spectrum applying the same procedure. The lower metallicity obtained by fitting the whole spectrum could be explained with a lack of flux (again due to calibration effects and/or to lack of lines in the emission models) around the 1 keV region. Another possibility (which is not mutually exclusive with the first one) is that the two-temperature model being used to fit the data is not a good representation of the real temperature distribution of the emitting plasma.

The possible lack of lines in current plasma emission codes in the region around 1 keV has for example been discussed by Jordan (1996), who makes explicit reference to the MEKA model (from which the MEKAL model used here has been derived by improving the Fe ionization balance and by adding a number of lines), concluding that *"in view of the large number of weak transitions not yet included in the emissivity codes it seems premature to attribute discrepancies between the observations and the predictions of the codes to non-photospheric abundances"*.

The dependence of derived abundances on the precise spectral interval being fit does *not* disappear if a model with all the abundances free to vary is used. Rather, it becomes more complicated because of the interplay between the various abundances, and because introducing a cut-off in the soft spectral region will make some specific abundances impossible to determine (notably nitrogen and oxygen). However, the resulting metallicities still strongly depend on the spectral interval being considered.

7. Discussion

The set of simulations presented here allow us to get some insight in the complex process of determining coronal abundances by global fitting of X-ray spectra, as well as to determine the expected range of uncertainty for the best-fit parameters as a function of spectrum statistics and of the intrinsic source metallicity. In addition, by giving an estimate of the range of variation in best-fit parameters that can be induced by a certain level of *statistical* error, it allows to estimate what can be the (approximate) effect of a certain level of *systematic* error present, for example, in the detector calibration or in the emissivity model.

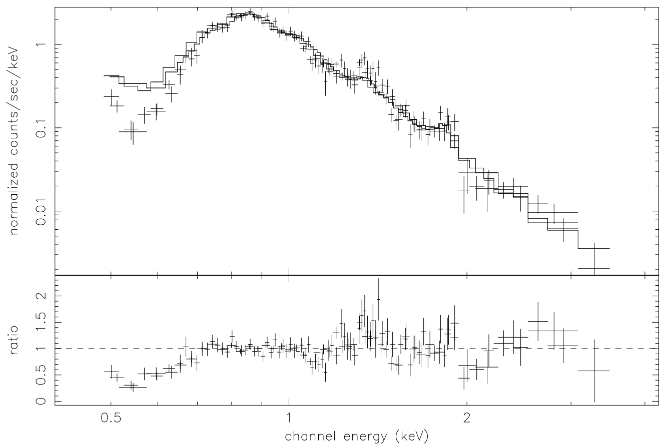

Fig. 11. The ASCA/SIS β Cet spectra, together with the best-fit model determined only considering the spectral range above 0.7 keV. Note that this model significantly over-shoots, as described in the text, the data in the softer region 0.5–0.7 keV.

The LECS performs better in constraning the intrinsic source metallicity than the SIS. This is due to the larger spectral range accessible, and in particular to the availability of a high signal-to-noise continuum region below 0.5 keV, with few and relatively weak lines, which appears to be more important, for spectroscopy of coronal sources, than the enhanced resolution of the SIS. In fact, as reported in Sect. 5.1, when we remove the spectral region below 0.5 keV from the LECS spectra, thus making its passband equal to the one of the SIS, the indetermination on the metallicity derived from spectra of the two instruments is similar, as it is the strong correlation between metallicity and emission measure ratio.

Some results from the simulations are remarkably different from what could have been expected. For example the cool component of the two-temperature source models is better constrained by the SIS than by the LECS (see Fig. 5). Naively, one would have expected that the softer response of the LECS should have led to smaller uncertainty on the cooler temperature. This example shows how the complex interactions of parameters in the fit process can lead to non-intuitive behavior and points, a posteriori, to the importance of basing the fit process on detailed simulation work.

Simulations can only provide a limited insight as they are done on the assumption that both the detector's calibration and the emissivity model are not affected by significant errors. However, they also show that even relatively small amounts of systematic errors can have a strong influence in the derived best-fit parameters. The statistical error of a 10 000 counts coronal spectrum in the peak (i.e. around 1 keV) is $\simeq 2.5\%$ per effective resolution element (obtained adding up the number of counts in the energy range corresponding to the FWHM resolution at 1 keV), for both the LECS and the SIS. This level of statistical uncertainty is sufficient to induce a 50% spread in the best-fit metallicity for SIS data at the 90% confidence level. Thus, similar levels of systematic errors, if present in the regions in which the spectrum has a high signal-to-noise, could induce comparable *systematic* shifts in the best-fit metallicity.

The analysis of real SIS spectra done in Sect. 6 points toward the likely presence of systematic effects due either to calibration uncertainties or to problems in the emissivity models or to the simplistic model used to fit the data (or to a combination of all the above effects), as shown by the strong dependence of the best-fit metallicity on the energy range used in the fit. In particular, our results on the soft sources β Cet and Capella could indicate a lack of predicted model flux in the region around 1 keV.

The present results point toward several items which should be considered critically when discussing coronal metallicities derived from low-resolution X-ray spectra. The most important are:

- Calibration uncertainties are likely to induce systematic effects in the determination of coronal abundances. As shown above, calibration uncertainties of a few percent could induce systematic shifts in the best-fit abundances of several tens of percent. Calibration uncertainties in the spectral region in which the signal-to-noise of stellar spectra is higher (around 1 keV) are potentially the most detrimental. Future instruments, such as XMM and AXAF, should thus pay particular attention to calibration in this spectral region (as well as in the region below 0.5 keV).
- Uncertainties in the plasma emissivity codes are as critical as detector calibration issues. Again, the region around 1 keV is the one which should be the made as reliable as possible. Flux deficits in this region will have a very strong influence in the derived source parameters, not in terms of larger confidence regions, but rather in terms of systematic shifts of best-fit values, due to the pivoting role of the region of the spectrum with the highest signal-to-noise ratio.
  This becomes even more critical if individual abundances are left free to vary, as elements like Ca and Ar, which have their K-complexes in the hard region of the spectrum, have their L-complex lines also in the $\simeq$ 1 keV region. Again, the fit process will be more influenced by the higher signal-to-noise L lines than by the better resolved but noisier K lines. Given the strong blending in the 1 keV region, uncertainties in few of the lines have a ripple-down effect on all abundances determined in the spectrum.
- Assuming too simplistic a model for the fit (as illustrated here by fitting power-law temperature distributions with two-temperature models) can also induce systematic shifts in the retrieved abundance. As the evidence from EUVE spectral analyses of coronal sources points toward complex plasma temperature distributions, it is not unlikely that two-temperature analyses of real coronal spectra are affected by similar effects. In this regard the LECS wide energy range provides improved diagnostic capabilities, thanks to the presence of two pivoting regions, one which is line-rich and one which is almost line-free.
  A hint of the possible inadequacy of the spectral model being used is, in the case of the LECS, the derivation of different best-fit abundances as a function of the adopted low-energy cut-off. As shown by the fit of the SIS data of Capella and β Cet discussed here, this may also be true with ASCA, although calibration uncertainties in the softer detector channels may also be playing a role there.

Acknowledgements. We would like to thank A. N. Parmar and N. S. Brickhouse for the useful discussions related to the subject of the present work. A. M., G. P. and S. S. acknowledge financial support from ASI (Agenzia Spaziale Italiana), MURST (Ministero della Università e della Ricerca Scientifica e Tecnologica), and GNA-CNR (Gruppo Nazionale Astronomia del Consiglio Nazionale delle Ricerche).

References

Ciaravella A., Maggio A., Peres G. 1997, A&A, in press,
Dotani T., Mitsuda K., Yamashita A. et al. 1996, ASCA Newsletter, 4
Drake S. A. 1996, in S. S. Holt, G. Sonneborn (eds.), Maryland conference on Cosmic Abundances, ASP, San Francisco, 215
Drake S. A., Singh K. P., White N. E., Simon T. 1994, ApJ, 436, L87
Eadie W., Drijard D., James F., Roos M., Sadoulet B. 1971, Statistical methods in experimental physics, 257, North-Holland
Jordan C. 1996, in S. Bowyer, R. F. Malina (eds.), Astrophysics in the extreme ultraviolet, IAU Colloquium 152, Kluwer, Dordrecht, p. 81
Maggio A., Favata F., Peres G., Sciortino S. 1997, A&A, submitted
Mewe R., Kaastra J. S., Liedahl D. A. 1995, Legacy, 6, 16
Parmar A. N., Martin D. D. E., Bavdaz M. et al. 1997, A&AS, 122, 309
Preibisch T. 1997, A&A, in press
Raymond J. C., Doyle J. G. 1981, ApJ, 247, 686

This article was processed by the author using Springer-Verlag LaTeX A&A style file *L-AA* version 3.